Noncollinear excitation of surface electromagnetic waves: Enhancement of nonlinear optical surface response

A. V. Andreev,[1] M. M. Nazarov,[1] I. R. Prudnikov,[1] A. P. Shkurinov,[1,*] and P. Masselin[2]
[1]*Department of Physics and International Laser Center, M. V. Lomonosov Moscow State University, Moscow 119992, Russia*
[2]*Laboratoire de Physico-Chimie de l'Atmosphère, CNRS UMR 8101, Université du Littoral, 145 avenue Maurice Schumann, 59140 Dunkerque, France*

(Received 30 April 2003; published 8 January 2004)

We excite several independent surface electromagnetic waves on a metallic surface by use of femtosecond laser pulses of different frequencies. Due to nonlinear plasmon interaction, optical radiations at frequencies 2ω, $\omega_1+\omega_2$, and $2\omega_2-\omega_1$ are generated (where ω_1 and ω_2 correspond laser beam frequencies). In the present paper we report experimental results and theoretical modeling of these multiphoton nonlinear optical effects from a metallic film sputtered onto a grating surface. The theoretical approach we use describes the multiphoton nonlinear optical effects in the presence of noncollinear interacting surface electromagnetic waves. In the experiments a sufficient enhancement of the nonlinear optical signals is achieved in the case where the incidence plane of light is parallel to the grating grooves.

DOI: 10.1103/PhysRevB.69.035403 PACS number(s): 73.20.Mf, 42.25.Bs, 42.25.Fx, 42.65.Ky

I. INTRODUCTION

The Surface Electromagnetic Wave (SEW) on metal-surface plasmon is a resonant coherent oscillation of conducting electrons at a surface.[1,2] A simple way to initiate a plasmon on a surface is to diffract laser beam on it. Under well-defined experimental conditions the reflection curve of the surface presents a minimum that correspond to the transfer of energy from the incoming beam to the plasmon. These remarkable minima are the well-established Wood anomalies of the diffraction grating. Wood first observed them in 1902 (Ref. 3) and since then they have been the subject of extensive research. These anomalies have undoubtedly resonant nature, because for a fixed experimental geometry the anomaly may be observed only at specific frequency ω, and reciprocally, for a fixed frequency of the incident light, the reflection anomaly is present at a defined angle of incidence θ or a defined azimuth angle φ. In this paper we denote the angle φ as the angle between the grating grooves orientation normal (reciprocal-lattice vector) and to the incidence plane (Fig. 1).

According to the dispersion relations[1] $K_{SEW}^{\omega}=\omega/c\sqrt{\epsilon_1\epsilon_2(\omega)/\epsilon_1+\epsilon_2(\omega)}$, where ϵ_1 and $\epsilon_2(\omega)$ are dielectric permittivity of the environment and of the metal, respectively, the value of the SEW's wave vector always exceeds the magnitude of the projection on the surface of the light wave vector at the same frequency. Hence, SEW's cannot interact with light on a flat surface (so-called nonradiating SEW) since there should be matching of the wave vectors to couple the light into SEW. For a light-SEW coupler such as a diffraction grating or prism the mismatching of SEW and light wave vectors is compensated.[4] On the grating SEW's can be excited by laser radiation, can absorb and reemit light, and thus, the result of SEW excitation (minimum in reflected light intensity) can be detected by optical methods.

The basic SEW properties are derived from the solution of Maxwell's equations.[1] The electromagnetic field of a plasmon decreases exponentially with the increase of the distance from the surface (direction of z axis in Fig. 1). However, in the direction along the surface (in the plane Oxy of Fig. 1) plasmons are relatively free to travel, and hence, they are truly propagating surface waves (concentrating the energy in a submicron layer near the surface) with a broad spectrum of eigen frequencies from $\omega=0$ to $\omega=\omega_p/\sqrt{2}$. For metals the plasma frequency ω_p is in the range of 10 eV. SEW selectively absorbs only a definite component of light polarization. In the case of a grating coupler, only the projection of light electric field on the reciprocal lattice vector q can interact with SEW.[5]

The SEW excitation leads to strong increase of the local electromagnetic field near the surface.[6] For the certain sets of parameters of the surface profile, the local-field intensity gain may reach several orders of magnitude. As a local-field gain we understand the ratio of the amplitude of the electromagnetic field on the surface to the amplitude of the incident light electromagnetic field. The giant local-field gain increases essentially the efficiency of the nonlinear optical processes that occur on the surface.[6]

The term ''nonlinear optical phenomena'' entered scien-

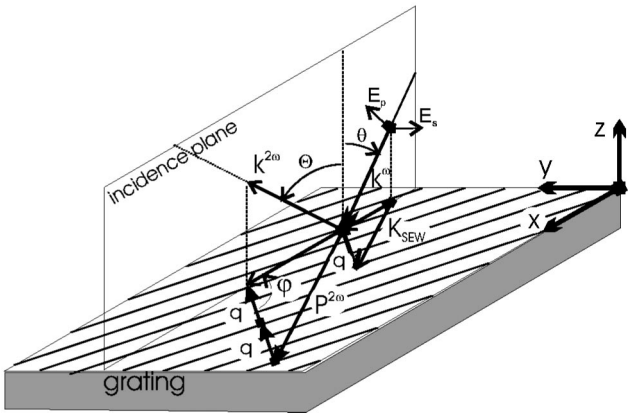

FIG. 1. Spatial wave vectors arrangement for SEW excitation and drawing of the experimental geometry in a reflection experiment on a grating for the SHG in arbitrary noncollinear scheme.

tific literature and became its integral part in the 1960s. It was understood as ''the effects with their history, characteristics and behaviors depending on the intensity of radiation.''[7,8] In the course of the development of nonlinear optics the term has got new additional meaning. The research of vector interaction of traveling[9–11] and localized plasmons[12] have formed recently the ''plasmon nonlinear optics'' when the interacting plasmon waves operate and govern nonlinear optical response of the system. At the same time the role of the field intensity is not denied. However, in this case the intensity of the resulting field can be of a secondary character, being the result of multiple interference of freely traveling, spreading plasmon waves. Similar description and behavior of nonlinear optical phenomena are observed in photonic crystals when the nonlinear optical response of the medium can be described as secondary phenomena based on coherent interference of vector electromagnetic fields.[13–16]

The simplest case of a nonlinear process—second optical harmonic generation (SHG) (Fig. 1) is a convenient tool to study the local-field enhancement. Following the history, in the general case the process of second optical harmonic generation from the surface was first described in the pioneering publication of Bloembergen,[17] later in Ref. 6 it was extended for the cases of multiphoton second- and third-order nonlinear optical processes. Coutaz and co-workers[18,19] and Simon[20] carried out successful experiments on the observation of the SHG efficiency on the silver sinusoidal gratings and compared the results with a flat metallic surface. A maximal second harmonic (SH) enhancement in four orders of magnitude has been achieved. In addition in Ref. 18 the authors demonstrated an important result: there exists an optimal value of the groove depth for which the SHG enhancement is maximal. The experimental data were analyzed on the basis of a theoretical model[21,22] that gives good qualitative agreement with the experiments. In 1994 Reinisch and co-workers[23] developed a useful simplified theoretical approach based on the coupled-mode formalism (modes of the fundamental and SH frequencies) where the SHG problem is solved in the framework of the linear diffraction theory. In the case of nonsinusoidal profile the modeling is complicated enough because it becomes important to take into account a large number of various spatial harmonics of the surface relief. This was realized in publications (Refs. 24,25) by introducing into the SHG description the spatial harmonics of the grating relief and their influence on the SHG efficiency in various diffraction orders. Among a variety of the theoretical works in this field we would like to note the publications of Kondratenko[26,27] who studied analytically SHG for an arbitrary polarization and grooves orientation in the case of sinusoidal grating.

The existing simplified theories of SHG by reflection from the metal surfaces with the modulated relief[26,27,29] fail to describe quantitatively the dependences observed experimentally even for second harmonic generation in reflection of metal film on nonsinusoidal substrate. We have to note that until now there is no analytical theory for the description of even the SHG on the periodic metallic surface of the arbitrary profile and grooves orientation. In Ref. 29 the case of

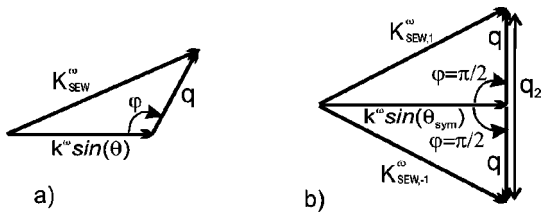

FIG. 2. Vectorial diagram of SEW excitations in the plane of grating surface. $\vec{K}_{SEW}$—SEW wave vector, $\vec{k}$—incident light wave vector, $\vec{q}$—reciprocal-lattice vector of grating, q_2—second spatial harmonic of the grating relief, φ—angle of grooves orientation, θ—incidence angle. (a) General noncollinear case, (b) special case of the symmetrical scheme when $\varphi = 90°$.

the sinusoidal relief was studied and mainly *p* polarization of the incoming beam was considered and it is supposed in the model that the grating might be described as a small perturbation parameter. The general case of SHG on the metallic grating (the grating is not supposed to be a small perturbation parameter) for the *p*-polarized incoming beam was presented in Ref. 30. The Raman-Nat diffraction on the gratings with the small groove period and depth, for three- and four-wave mixing processes has also been discussed.[31]

The absence of complete theory leads to the formation of the stable opinion that for an efficient SHG one should use the surface with the sinusoidal profile. It is quite reasonable, if one takes into account that the sinusoidal relief is optimal for the achievement of the total suppression of the specular reflection at the fundamental frequency. However, in publications (Ref. 24) the authors supposed, that the harmonics of the relief might selectively enhance the nonlinear optical process in various diffraction orders. For instance, the second harmonics of the spatial relief have strong influence on the efficiency of the SHG in the specular reflection, but it slightly modifies the SHG intensity in ± 1 diffraction orders. In earlier work[32] we already studied the dependence of the SHG efficiency on the amplitude of the spatial harmonics of the relief. The overwhelming majority of the experimental and theoretical works on SEW excitation and interaction were carried out using the sinusoidal profile and collinear geometry. For the nonlinear surface plasmon optics and spectroscopy the use of nonsinusoidal grating profile together with the noncollinear geometry of SEW excitation-interaction (see below) are more preferable. The SEW excitation by *s*-polarized laser light[33–35] leads to the excitation of two noncollinear SEW's and their coupling through diffraction [Fig. 2(b)].

The paper is organized as follows: In Sec. II different geometries of SEW excitation and their interaction on the grating are presented. The advantages of symmetrical noncollinear scheme of SEW excitation by *s*-polarized light are outlined. Several types of multiplasmon surface nonlinear processes are considered. In Sec. III theoretical formalism which can describe arbitrary experimental geometry and surface profile is presented. The brief description of the experimental setup used in the experiments and the samples preparation routine are described in Sec. IV. Measurements of the efficiency and optimal geometry of various nonlinear processes such as SHG, sum-frequency generation (SFG), four-

wave mixing (FWM) are presented in Sec. V. The validity of the theory is shown on the example of comparison with the experimental measurements of specular reflection and SHG efficiency for several values of φ as a function of incidence angle θ. In Sec. VI the main conclusions of the paper are presented.

II. NONCOLLINEAR SURFACE ELECTROMAGNETIC WAVES EXCITATION AND THEIR INTERACTIONS

In this section we describe the basic terms of the plasmon optics that will be used in the paper. Two stages should be distinguished: excitation of one (or several) SEW's (Fig. 2) and their interaction (Fig. 3). The geometries of these processes may be different.

A. Different schemes of surface electromagnetic wave excitation on the grating

The scheme of SEW excitation may be collinear and noncollinear. In the widely used collinear geometry ($\varphi=0,\pi$) light wave vector is parallel to the reciprocical-lattice vector q. The p-polarized optical wave incoming on the grating transfers into the SEW and the SEW runs in the plane of incidence. All other geometries are noncollinear (Figs. 1 and 2).

Let us assume that in the case of p polarization, the electric field $\boldsymbol{E}$ is in the plane of incidence, thus $E_y=0$, $H_x=H_z=0$. The cartesian unit vector directions are defined in Fig. 1. For an arbitrary geometry phase matching condition for SEW excitation on the grating is $\vec{k}_t^{\omega}+n\vec{q}=\vec{K}_{SEW}^{\omega}$ [Fig. 2(a)] where n is an integer. The real part of $\vec{K}_{SEW}^{\omega}$ participates in phase matching. In cartesian coordinate system it is

$$k_{t,x}+q_x=K_{SEW,x};\quad q_y=K_{SEW,y}, \tag{1}$$

where $q_x=(2\pi/d)\cos(\varphi)$, $q_y=(2\pi/d)\sin(\varphi)$, $k_{t,x}=(\omega/c)\sin(\theta)$, $q_z=k_{t,z}=k_{t,y}=K_{SEW,z}=0$. Here the coordinate system (xz plane) is linked to the incidence plane of light, z is normal to the averaged surface, y is normal to the incidence plane (Fig. 1), d is a grating period, n is the order of diffraction. For the definite grating d is a fixed value and there are three variable parameters to achieve SEW resonance—θ,φ,ω.

If in noncollinear geometry the grating grooves are parallel to the incidence plane, that is, $\varphi\approx 90°$ (Ref. 10) [Fig. 2(b)] the experimental configuration has mirror symmetry with respect to the incidence plane. This configuration is further referred to as ''symmetrical scheme.'' However, some authors call this configuration ''s-polarization case'' because s polarization of the incoming beam transfers into the p-polarized plasmon wave. Note that the collinear scheme ($\varphi=\pi l$, where l is an integer value) is also symmetrical. All interactions occur here in one direction but in general it does not give any advantages in comparison with the arbitrary scheme.

Here we assume that in the case of s polarization, the electric field is normal to the incident plane (x,z), i.e., $E_x=E_z=0$, and the magnetic field is in this plane ($H_y=0$). In this case vector q is directed along y direction $q=q_y$. As

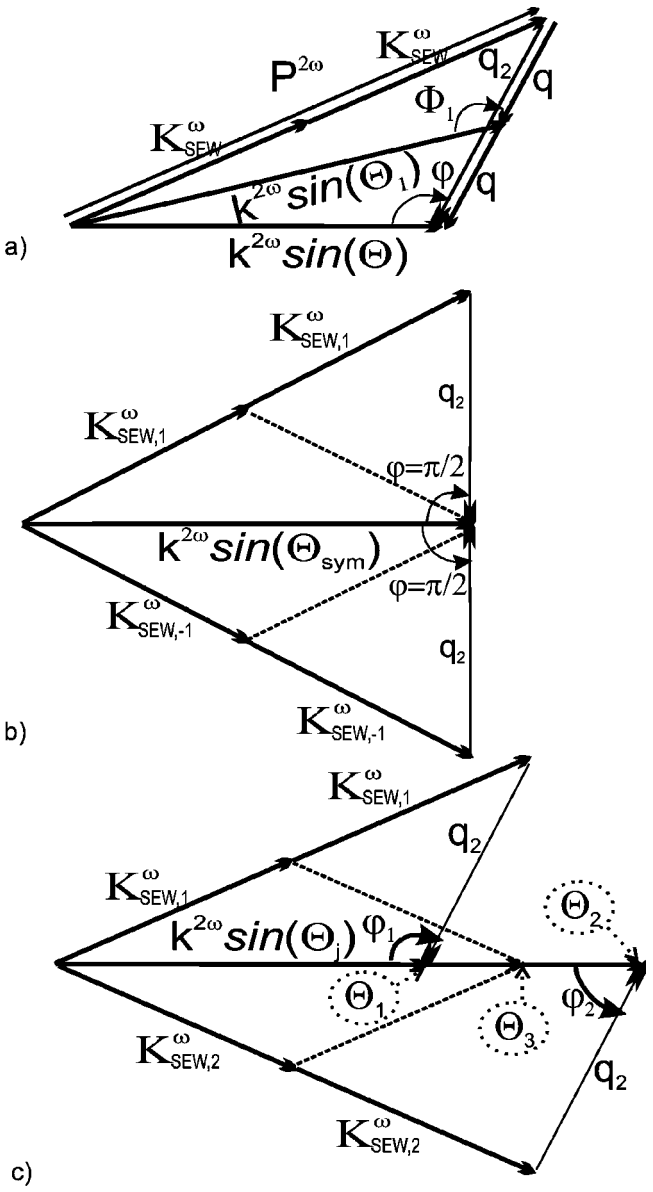

FIG. 3. Drawing of the vectorial diagram presented in the plane of grating surface for degenerated SEW interaction for SHG. $\vec{K}_{SEW}^{\omega}$—SEW wave vector, $\vec{P}^{2\omega}$—nonlinear polarization, $\vec{k}^{2\omega}$—wave vector of second optical harmonic, Θ—angle of light radiated from the surface, q_2—second spatial harmonic of the grating surface relief. (a) A general case of collinear interaction, (b) combined collinear or noncollinear interaction in symmetrical scheme when $\varphi=90°$, (c) separate collinear or noncollinear interaction.

applied to various nonlinear optical effects, during the recent years we studied experimentally several schemes of SEW excitation and their further interaction. For the first time, we used the noncollinear scheme for the excitation of surface electromagnetic waves on the grating in Ref. 32. In this work we give emphasis to the studies of various nonlinear effects associated with their local-field enhancement in the presence of running and interacting SEW's excited in the symmetrical scheme. The characteristic minima in specular reflection from the grating for s-polarized incoming light was first ob-

served in 1967 (Ref. 36) and later was comprehensively described in theory in Refs. 26,33–35. In symmetrical geometry of SEW excitation the amplitude of the *p* component of the SEW electric field is determined only by the amplitude of the *s* component of the incoming electric field.[27] The phase matching conditions for the SEW excitation are fulfilled both for positive and negative values of the reciprocal lattice vector $\vec{q}$, and accordingly two SEW's are excited in different directions simultaneously [Fig. 2(b)]. Moreover, one SEW is diffracted to the other one: $\vec{K}^{\omega}_{SEW,1}+2q=\vec{K}^{\omega}_{SEW,-1}$. The phase matching condition for this process is fulfilled automatically in the symmetrical scheme. The presence of the second spatial harmonics of relief makes this noncollinear SEW coupling more efficient [Fig. 2(b)].

B. Schemes of multiple surface electromagnetic waves interaction

The term SEW interaction concerns the description of the geometries of interaction of several SEW's. It can also be collinear or noncollinear. For the experiments that use one beam interacting SEW wave vectors are collinear [Fig. 3(a)], except for the symmetrical scheme [see Fig. 3(b)], where $K^{omega}_{SEW,1}$ interacts with $K^{omega}_{SEW,-1}$. In most of the experiments with several beams/frequencies as shown in Fig. 4, noncollinear interaction is added. For the realization of noncollinear SEW's interaction, at least one of the interacting SEW's must be excited using noncollinear geometry ($\varphi \neq \pi l$). And vice versa, SEW's excited in collinear geometry interact only collinearly. As SEW propagation length at optical frequencies is restricted by several hundreds of microns,[28] which is comparable with the focused laser beam spot on the grating surface, the noncollinear scheme of SEW interaction does not reduce the interaction length considerably.

The simplest result of SEW interaction is SHG. This process has the following scheme: two SEW's originate the polarization at doubled frequency $\vec{K}^{\omega}_{SEW}+\vec{K}^{\omega}_{SEW}=\vec{P}^{2\omega}$ due to nonlinear surface susceptibility $\chi^{(2)}_s$, $P^{2\omega}\sim(\chi^{(2)}_s I^{\omega})^2$. This process is rather weak (typically $(I^{2\omega})/(I^{\omega})\approx 10^{-18}-10^{-12}$). In centrosymmetric media it is allowed only at the surface and it requires high local-field intensities. Thus, SHG from metal surface is well observable only if light is transformed into SEW. $\vec{P}^{2\omega}$ cannot straightforwardly radiate into the environment because of phase mismatching, but diffraction orders of $\vec{P}^{2\omega}$ can be radiated on the grating.

Let us assume that the Θ indicates the angle of direction of emission out of the grating surface relative to the surface normal, Φ indicates azimuth angle of emission. It is easy to show that the direction Θ of the second diffraction order of polarization at doubled frequency $\vec{P}^{2\omega}$ coincides with specular reflection direction θ of the wave at the fundamental frequency: $\vec{P}^{2\omega}-2\vec{q}=\vec{k}^{2\omega}_t$, $\Theta=\arcsin(k^{2\omega}_t)/(2\omega/c)=\theta$, $\Phi=\varphi$ (Figs. 1 and 2). First order of diffraction of $P^{2\omega}$, radiated at angles Θ_1,Φ_1 is also observed both in experiment and in theory and it can be even more intensive than the second order, but it is less convenient for application because $\Phi_1 \neq \varphi$ (except the case $\varphi=\pi l$) and SHG direction does not lie in the incidence plane so we will not discuss such processes in this paper.

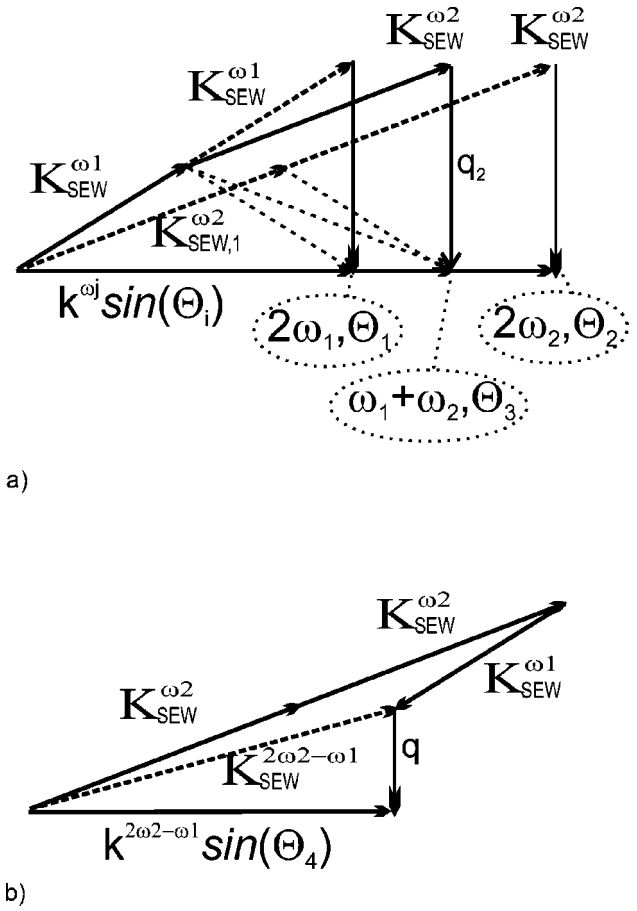

FIG. 4. Vectorial diagram of nondegenerated SEW interaction in symmetrical scheme. $\vec{K}^{\omega i}_{SEW}$—SEW wave vector at corresponding frequency, $\vec{k}^{\omega j}$—wave vector of resulting wave, Θ—angle of light radiation corresponding frequency, mirror symmetrical lower parts of diagram are not presented on the drawing. (a) Three different second-order nonlinear processes, SHG_1, SHG_2, and SFG, radiated under different angles Θ_i, (b) resulting wave on the four-wave mixing frequency $2\omega_2-\omega_1$ can also be a surface type one.

The presence of sufficient second harmonics of spatial relief peculiar to the nonsinusoidal grating profile[35] can considerably increase nonlinear processes efficiency in the case of noncollinearly excited SEW's. In both the experiment and the theory we consider shallow gratings and second order of diffraction is much less efficient than the first one. As it was shown above, in the general case of SEW enhanced SHG on the grating, SHG wave is reradiated through the second order of diffraction on the reciprocal-lattice vector $\vec{q}$. Thus, the appearance of the second spatial harmonics $\vec{q}_2$ in the Fourier spectrum of the grating groove profile leads to a nonlinear polarization radiation through the first diffraction order and to a considerable enhancement of SHG (and SFG as well) efficiency in all geometries[37](Fig. 3). In symmetrical scheme, $\vec{q}_2$ plays one more important role [see Fig. 2(b)]. Two originated noncollinear SEW's become coupled through scatter-

ing on $\vec{q}_2$ (in other words Bragg reflection condition from grating grooves is fulfilled for both SEW's) and a standing wave may be formed in *y* direction. Hence, for the grating with an optimized spatial profile of the surface in the symmetrical scheme one can achieve much higher local electromagnetic field then in other schemes.

To separate the contribution of noncollinear SEW interaction in SHG, we carried out the experiment on degenerated SFG, from two laser beams[9] [see Fig. 3(c)]. Two SEW's were independently excited in one point of the grating surface but they run in different directions. Experimentally we were able to separate spatially SHG waves originated from collinear (Θ_1 and Θ_2) and noncollinear (Θ_3) interacting SEW's [Fig. 3(c)] and we have shown that noncollinear channel can be more efficient, than the collinear one. Further on we performed our experiments in the symmetrical scheme—the most efficient for nonlinear signal enhancement.

As this paper is mainly devoted to the discussion of nonlinear optical effects resulting from the interaction of the noncollinear SEW's we present the drawings related to the general case of multiphoton and multibeam interactions, such as SHG [Fig. 3(b)], SFG [Fig. 4(a)], and FWM [Fig. 4(b)]. In the example of SFG and FWM experiments we demonstrate the efficiency of the noncollinear SEW interactions in the nondegenerated frequency cases (see Fig. 4).

For multibeam configuration, the SEW's are excited by laser beams according to the phase matching condition $\vec{k}^{\omega}_{t,i} + n_i\vec{q} = \vec{K}^{\omega}_{SEW,i}$, where $i = 1,2,\ldots$ denote beam numbers, n_i is the diffraction order. $\vec{K}^{\omega}_{SEW,i}$ is the corresponding SEW's wave vector [Figs. 3(c) and 4]. Only $\vec{q}$ direction is fixed for all *i* values, so $\omega_i, \varphi_i, \theta_i$ can be varied in order to optimize the properties of the process of under study.

The generated SEW's radiate the electromagnetic waves at combinational optical frequencies if the correspondent phase matching condition is fulfilled and SEW's at fundamental frequencies ω_1 and ω_2 are overlapped in space and time. The directions of the generated waves Θ_j, Φ_j (for our case $j=1$ is $2\omega_1$, $j=2$ is $2\omega_2$, $j=3$ is $\omega_1+\omega_2$, $j=4$ is $2\omega_2-\omega_1$) are determined by the following relations between interacting SEW wave vectors:

$$\vec{K}^{\omega_1}_{SEW,1} + \vec{K}^{\omega_2}_{SEW,2} + n_3\vec{q} = \vec{k}^{\omega_1+\omega_2}_{t,3} \quad \text{for nondegenerated SFG,}$$

$$2\vec{K}^{\omega_2}_{SEW,2} - \vec{K}^{\omega_1}_{SEW,1} - \vec{q} = \vec{k}^{2\omega_2-\omega_1}_{t,4} \quad \text{for FWM process.}$$

Figure 4 shows the vectorial layout for nondegenerate noncollinear SFG [Fig. 4(a)] and FWM [Fig. 4(b)]. The angle of radiation is calculated as $\Theta_j = \arcsin(k_{t,j}/\omega_j/c)$. For the sake of simplicity all beams in our configuration are in one plane of incidence, so $\Phi_j = \varphi_i = \varphi$. The proper choice of angles φ_i and θ_i leads to the simultaneous fulfillment of phase matching conditions for SEW's at all frequencies of interacting waves (Fig. 13).

In any nonlinear optical process on the grating the symmetrical scheme is advantageous from the point of view of increasing the number of channels of local-field enhancement of a definite process. For instance, for FWM instead of one channel in collinear geometry, we obtained eight parallel channels, when SEW's with two different frequencies were excited simultaneously both in symmetrical schemes. Analogously, SEW on the grating may be applied for five and more wave mixing nonlinear processes. Finally, we would like to note that the excitation of SEW at the resulting nonlinear frequency is possible only in noncollinear geometry of SEW interaction (because of nonlinear SEW dispersion relation). When the resulting frequency lies in visible or IR range of spectrum, the excitation of SEW at the resulting frequency may considerably enhance the efficiency of the nonlinear process. In our experiment such situation took place only for FWM process.

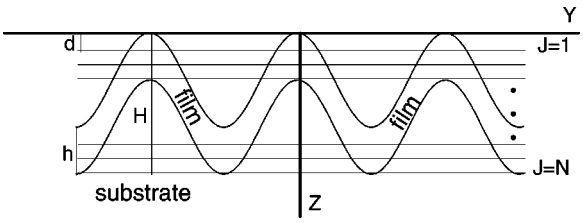

FIG. 5. Geometry analyzed in the present paper and fragmentation on layers for the model. The metal film has a $\sin^2$ profile with period *T*, amplitude $H' = H - h$, and the "thickness" of the gold layer *h*.

III. THEORY

In this section we outline the derivation of the numerical technique that allows us to compute the field that is localized and scattered out of a grating surface. For the quantitative description of the scattering of the incoming laser beam on the periodic surface relief we use a recurrence method. This approach was first developed by Darwin in his pioneering publication[38] devoted to the theory of dynamic x-ray diffraction in crystals. Figure 5 shows the layout of the system under study, some of the notations, and the coordinate system. Let us assume that the arbitrary periodic relief in *z* coordinate direction is a superposition of the sandwiched *N* layers that are parallel to the $z=0$ plane and of thickness *d* for each (Fig. 5). The total height of the relief is $H = Nd$. We suppose that all the layers are separated by the vacuum line cracks with the thickness of Δ, and $\Delta \to 0$. At the beginning, we would like to solve the problem of scattering of a monochromatic vectorial field on the single individual inhomogeneous layer. Let us find the solution of the wave equation for the electric field presented in the integrated form[39]

$$\vec{E}(\vec{r},t) = -\frac{1}{4\pi c^2}\frac{\partial^2}{\partial t^2}\int \chi(\vec{r}\,')\frac{\vec{E}\left(\vec{r}\,', t-\frac{R}{c}\right)}{R}d\vec{r}\,' + \frac{1}{4\pi}\int \chi(\vec{r}\,')\,\mathrm{grad}\,\mathrm{div}_{\vec{r}}\frac{\vec{E}\left(\vec{r}\,', t-\frac{R}{c}\right)}{R}d\vec{r}\,' + \vec{E}^{i}(\vec{r},t) \tag{2}$$

where $R=|\vec{r}-\vec{r}'|$ and $\vec{E}^i(\vec{r},t)$ is the incoming field directed from vacuum ($z<0$) to the layer, $\chi(\vec{r})$ polarizability of the inhomogeneous layer. Integration in Eq. (2) is carried out over the whole layer $-\infty<x'<\infty$, $-\infty<y'<\infty$, $0\leqslant z'\leqslant d$. Equation (2) may be obtained as a result of the solution of Maxwell equations with the use of the retarded potential technique.[40] The polarizability $\chi(\vec{r})$ and the field incoming on the layer may be represented in the form

$$\chi(\vec{r})=\sum_n \chi_n \exp(iqny),$$

$$\vec{E}^i(\vec{\rho},z,t)=\sum_m \vec{E}^i_m \exp(i\vec{\kappa}^0_{\parallel}\cdot\vec{\rho}+iqmy+i\kappa^m_z z-i\omega t), \quad (3)$$

where $\vec{\rho}=(x,y)$, $\vec{\kappa}^0_{\parallel}=(\kappa^0_x,\kappa^0_y)$, $\kappa^m_z=\sqrt{\kappa_0^2-(\kappa^m_y)^2-(\kappa^0_x)^2}$, $\kappa^m_y=\kappa^0_y+mq$, $\kappa_0=2\pi/\lambda$, $q\equiv q_y=2\pi/T$ reciprocal-lattice vector. Here we assume, for the sake of definiteness, that the reciprocal-lattice vector q is always aligned with the Y axis, $q=q_y$ (see Fig. 5). In the mean time, the wave vector of the incoming wave k_0 is directed both at arbitrary incidence and azimuth angles. Let us suppose that the thickness of the layer is small enough in order to make the following assumptions:

(1) The amplitude of the scattered to the vacuum field ($z<0$) is much less than the amplitude of the incoming one. It means that the boundary conditions on the surface of the layer ($z=0$) may be presented in the following form:

$$E_{x,y}(\vec{\rho},0,t)=E^i_{x,y}(\vec{\rho},0,t)$$

$$[1+\chi(\vec{r})]E_z(\vec{\rho},0,t)=E^i_z(\vec{\rho},0,t).$$

(2) The field inside the layer depends weakly on the z coordinate: $\vec{E}(\vec{\rho},z,t)\approx\vec{E}(\vec{\rho},0,t)$.

Taking into account both these assumptions the field scattered into vacuum has the following presentation:

$$\vec{E}^s(\vec{\rho},z\leqslant 0,t)=\sum_p \vec{E}^s_p \exp(i\vec{\kappa}^0_{\parallel}\vec{\rho}+iqpy-i\kappa^p_z z-i\omega t), \quad (4)$$

where

$$(\vec{E}^s_p)_x=\frac{id}{2\kappa^p_z}\sum_m \{[\kappa_o^2-(\kappa^0_x)^2]\chi_{p-m}(\vec{E}^i_m)_x - \kappa^p_y\kappa^0_x\chi_{p-m}(\vec{E}^i_m)_y+\kappa^p_z\kappa^0_x\xi_{p-m}(\vec{E}^i_m)_z\},$$

$$(\vec{E}^s_p)_y=\frac{id}{2\kappa^p_z}\sum_m \{-\kappa^p_y\kappa^0_x\chi_{p-m}(\vec{E}^i_m)_x +[\kappa_o^2-(\kappa^p_y)^2]\chi_{p-m}(\vec{E}^i_m)_y+\kappa^p_z\kappa^p_y\xi_{p-m}(\vec{E}^i_m)_z\},$$

$$(\vec{E}^s_p)_z=\frac{id}{2\kappa^p_z}\sum_m \{\kappa^p_z\kappa^0_x\chi_{p-m}(\vec{E}^i_m)_x+\kappa^p_z\kappa^p_y\chi_{p-m}(\vec{E}^i_m)_y +[\kappa_o^2-(\kappa^p_z)^2]\xi_{p-m}(\vec{E}^i_m)_z\},$$

$$\chi(\vec{r})/[1+\chi(\vec{r})]=\sum_n \xi_n \exp(iqny).$$

Here ξ_n is a Fourier coefficient. A similar expression can also be obtained for the field, transmitted through the layer to vacuum, $\vec{E}^t(\vec{\rho},z\geqslant d,t)$. With the use of Eq. (4) the relations between scattered $\vec{E}^s(\vec{\rho},z=0,t)$, transmitted $\vec{E}^t(\vec{\rho},z=d,t)$, and incoming $\vec{E}^i(\vec{\rho},z=0,t)$ fields can be written in the matrix form:

$$\hat{\Psi}^s=\hat{s}\hat{\Psi}^i$$
$$\hat{\Psi}^t=\hat{\tau}\hat{\Psi}^i, \quad (5)$$

where

$$\hat{\Psi}=\begin{pmatrix}\vdots\\ \hat{\Psi}_1\\ \hat{\Psi}_0\\ \hat{\Psi}_{-1}\\ \vdots\end{pmatrix}$$

column matrix consists of the amplitudes of the Bloch waves for the fields

$$\hat{\Psi}_m=\begin{pmatrix}(\vec{E}_m)_x\\ (\vec{E}_m)_y\\ (\vec{E}_m)_z\end{pmatrix}.$$

Formulas (4) and (5) describe the process of scattering of the monochromatic vectorial field (3) with any arbitrary polarization for an arbitrary angle of incidence θ. It also permits us to introduce the variation of the azimuth angle φ. Let us consider an arbitrary layer j inside the relief (Fig. 5). We suppose that the enumeration of the layers begins from $z=0$ plane and for the first layer $j=1$. We will express the fields inside the vacuum gap just in front of the jth layer as $\hat{\Psi}^{s,t}_j$. Thus, according to Darwin's procedure we may obtain the general recurrence relations for the fields:

$$\hat{\Psi}^t_j=\hat{\tau}_{j-1}\hat{\Psi}^t_{j-1}+\hat{\overline{s}}_{j-1}\hat{\Psi}^s_j, \quad (6a)$$

$$\hat{\Psi}^s_j=\hat{s}_j\hat{\Psi}^t_j+\hat{\overline{\tau}}_j\hat{\Psi}^{\hat{s}}_{j+1}, \quad (6b)$$

where $\hat{\overline{s}}_j$, $\hat{\overline{\tau}}_j$ matrix elements may be obtained in the same way as $\hat{s}_j$, $\hat{\tau}_j$, but for the case when the field impinges on the reverse side of the layer. In Eq. (6) the combination $\hat{\tau}_{j-1}\hat{\Psi}^t_{j-1}$ describes the field transmitted by the $(j-1)$th layer, the combination $\overline{s_{j-1}}\hat{\Psi}^s_j$—rescattering of the field already scattered on the $(j-1)$th layer, $\hat{s}_j\hat{\Psi}^t_j$ determines the

scattering of the transmitted field on the jth layer and, finally, $\overline{\tau_j}\hat{\Psi}^s_{j+1}$ is the value of the scattered field transmitted by the jth layer. Equations (6) deliver the complete solution to the problem of the linear reflection of the vectorial electromagnetic wave field from the surface grating for both arbitrary azimuth angles and incidence angles. To demonstrate this, we introduce the following matrix $\hat{R}_j$: $\hat{\Psi}^s_j=\hat{R}_j\hat{\Psi}^t_j$, that describes the scattering process for the periodic relief of height $H_j=d(N+1-j)$, which is a lower part of the entire relief. Equations (6) allow one to obtain the following recurrence formula[41] for the calculation of the $\hat{R}_j$ values:

$$\hat{R}_j=\hat{s}_j+\overline{\hat{\tau}_j}\hat{R}_{j+1}(\hat{1}-\overline{\hat{s}_j}\hat{R}_{j+1})^{-1}\hat{\tau}_j. \tag{7}$$

Recurrence relations (7) allow one to determine the matrix $\hat{R}_1$ that describes scattering from the whole grating of height H. First, with the use of the common Fresnel formula we should calculate the matrix $\hat{R}_{N+1}$ that determines reflection from the homogeneous semi-infinite half-space $z>H$ (Fig. 5). Then, on the basis of the recurrence formula (7) we obtain the $\hat{R}_1$ values. We would like to point out that the decomposition of the periodic relief on the separate layers was also used by Barabenkov *et al.*[42] that resulted in the first-order differential Rikatti equation for the field amplitudes. Compared with their approach, the recurrence relations approach (6) is a general one, because it is not limited by the consideration of the field derivative of the first order only. The above-described algorithm may also be used for the calculation of the local intensity of the total wave field $I(\vec{\rho},z)$ inside the surface relief. Moreover, the algorithm can be easily generalized for the description of the nonlinear scattering effects in the periodic inhomogeneous media. It may be achieved by the addition into the right side of Eq. (6a) of the wave field $\hat{f}^t_{j-1}$ originated as a result of the nonlinear scattering inside the $(j-1)$th layer and then incoming on the jth layer. Simultaneously, into the right side of Eq. (6b) one should add the field of the nonlinear optical response $\hat{f}^s_j$ appearing in the jth layer. The sources $\hat{f}^{t,s}_j$ should be calculated in the given pump field approximation and supposed to be known. Thus, the problem comes to the resolution of the inhomogeneous system of the recurrence equations in order to find the field of the nonlinear response $\hat{\Psi}^s_1$ under the condition $\hat{\Psi}^t_1\equiv\hat{0}$. Here we should take into account a specific distribution of the sources of nonlinear response inside a sample.

IV. EXPERIMENTAL SETUP AND THE SAMPLE PREPARATION

A. Experimental details

Figure 6 presents a schematic drawing of the experimental setup. The laser sources (not shown here) are described in detail in our previous publications, e.g., Refs. 13,14. We used a laser system consisting of a femtosecond mode-locked Ti:sapphire laser to seed a regenerative amplifier (RegA) and an optical parametrical amplifier (OPA). A part of RegA laser

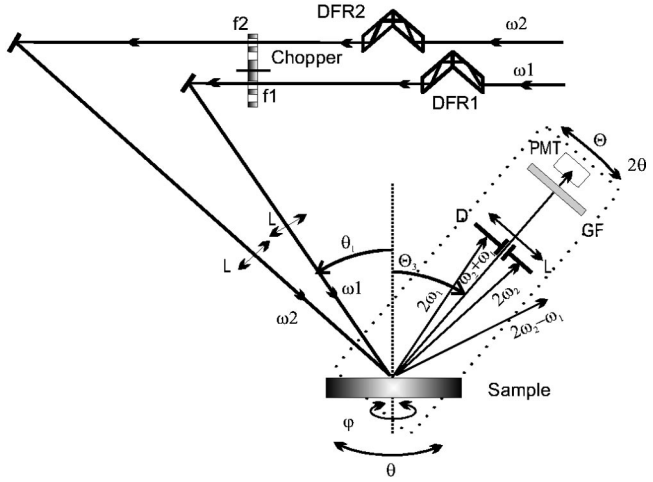

FIG. 6. Optical scheme of the experimental setup with two frequencies ω_1 and ω_2. DFR1, 2 double Fresnel rhombus; L—lenses; GF—glass filter; PMT—photomultiplier; D—diaphragm; θ—angle of incidence; Θ—angle of radiation; φ—angle of groove orientation, f_1 and f_2 are the frequencies of the modulation of the first and the second optical channels.

radiation is seeded into OPA to produce tunable light that is used as ω_2 beam in SFG ($\omega_{SF}=\omega_1+\omega_2$) and FWM ($\omega_{FWM}=2\omega_2-\omega_1$) processes. Our OPA produces tunable light in the range of 500–750 nm. Another part of the RegA output forms the beam ω_1, necessary for the SFG and FWM signals generation. The central wavelength of the spectrum of the ω_1 pulse is variable in the range of 780–825 nm.

The temporal overlapping of ω_1 and ω_2 pulses is achieved by the use of a delay line. A double Fresnel rhombus (DFR) provides the possibility to rotate the angle of polarization plane of both ω_1 and ω_2 beams. We use linearly polarized beams with the fraction of residual (orthogonal) component as less as 10^{-3}. Typically, for both beams averaged power was 10 mW, repetition rate 200 kHz, pulse duration 300 fs, spectral width 12 nm (chirped pulses).

The sample (grating) was mounted on one rotary part of the goniometer in order to vary and align the incident angles. The registration system is held on another rotary part of the goniometer. The incident angle θ_1 is counted from the position of normal incidence of ω_1 beam on the sample. Additionally to a collimating lens (L) the registration system consists of a diaphragm (D), and a set of shortpass glass filters (GF) to reject scattered light at frequencies ω_1 and ω_2. The signal registration is realized with Hamamatsu R 4220P photomultiplier tube (PMT) connected to a lock-in-amplifier EEG-5110 (EG&G) for synchronous selective detection. There is a chopper in both beam path. It chops ω_1 and ω_2 beams at frequencies $f_1\sim628$ Hz and $f_2\sim383$ Hz, respectively. The frequency of detection is chosen as f_1, f_2, or $f_1+f_2=1011$ Hz, depending on what kind of signal (SHG1, SHG2, SFG, or FWM) is measured.

A part of the experiments concerning SHG and specular reflection (R) measurements were done on a similar setup[9] with one (also Ti:sapphire) laser source. In that case typically averaged power was 100 mW, repetition rate 100 MHz, pulse duration 100 fs, tuning range 730–850 nm, spectral width 12

TABLE I. Diffraction gratings parameters.

Sample	H^{a}	$H^{ef\,b}$	T^{c}	h^{d}	$f_1{}^{e}$	$\varphi_1{}^{f}$	f_2	φ_2	f_3	φ_3
B2	120	48	1140	50 (Ag)	18	−2,4	5,4	2,2	2,6	−3,8
M9	130	100	1150	30 (Au)	31	3	20	1,6	8	0
T6	135	100	1120	35 (Au)	61	5	17	2,4	0	0

[a]H (nm)—total amplitude of the grating.
[b]H^{ef} (nm)—efficient amplitude of the grating.
[c]T(nm)—period of the grating.
[d]h(nm)—thickness of the metal layers.
[e]f_1, f_2, f_3(nm)—amplitudes of the first, second, and third harmonics of the spatial relief.
[f]$\varphi_1, \varphi_2, \varphi_3$(rad)—phases of the first, second, and third harmonics of the spatial relief.

nm (transform-limited pulses). Reflection and SHG were measured simultaneously using dichroic mirror and two detectors for fundamental and doubled frequencies. To measure R in (θ, φ) space [Fig. 10(a)] we used highly divergent $(\Delta\theta = 15^0)$ monochromatic laser beam and charge coupled device camera as a detector.

B. Diffraction grating preparation

The holographic methods for fabrication of grating structures with periodic surface profiles by Fourier synthesis allow controlled superposition of spacial harmonics. In our work the gratings on the quartz substrates were fabricated using the standard holographic procedure. First, the exposition of photoresist layer as performed by He-Cd laser. After the development of photoresist the grating mask was formed. Then the grating pattern is transferred into glass by ion etching process. The groove profile of the grating after this procedure is usually close to trapezoidal which was confirmed by observation of the groove profile by an electron microscope. After the ion etching process the glass samples were annealed in a furnace at the temperature near glass softening temperature. This procedure allows us to obtain the gratings with profiles close to sinusoidal. Then gold or silver metal film with the thickness of 30–50 nm was deposited on the grating surface.

C. Diffraction grating characterization

We would like to comment that in this paper we keep the names of the grating samples (e.g., B2, M9, T6) as they were given by technologists and we believe it would be convenient for the comparison of the results in the papers published earlier or later. For the sample characterization we used two alternative mutually additive methods:

(1) In the first method, the profiles of the gratings were investigated with the scanning tunneling (STM) and atomic force (AFM) microscopes. The parameters of the diffraction grating samples used in the experiments are presented in Table I. In Fig. 7 we show the profiles of the sample T6. In Table I we indicated also the relative amplitudes and phases of the harmonics of the spatial relief.

$$z(x) = \sum_{I=1}^{3} f_i \sin\left(\frac{2\pi}{T}x + \varphi_i\right), \quad H^{ef} \approx 2\left(\sum_i f_i\right),$$

$$H = H^{ef} + h. \tag{8}$$

(2) The other characterization method used was the fit of the $R(\theta, \varphi)$ dependencies by numerical calculations (Figs. 8 and 9) using the above-described theory. In the numerical calculations amplitude and depth of SEW resonance critically depends on film thickness, groove height, and shape.

V. EXPERIMENTAL RESULTS AND DISCUSSION

A. Linear and nonlinear reflectivity angular dependencies

We display in Figs. 8 and 9 the experimental and related to them computer simulation results on specular reflection $R(\theta)$, (a) at the fundamental frequency and the reflected SHG $I_{SHG}(\theta)$, (b) Fig. 8 describes the angular behavior of

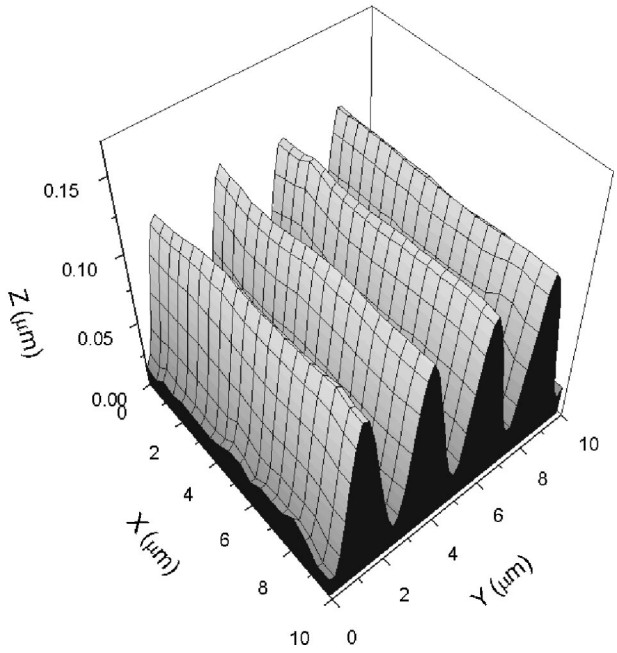

FIG. 7. 3D image of metal grating surface for the sample T6 obtained with the atomic force microscope.

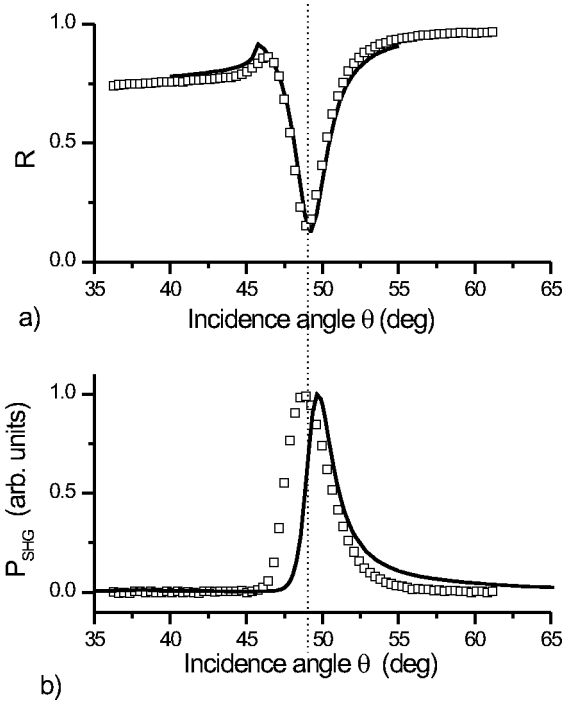

FIG. 8. Linear reflection coefficient R (a) and SHG power P_{SHG} (b) versus the angle of incidence θ of the radiation with the wavelength $\lambda = 780$ nm in symmetrical ($\varphi = 90°$) scheme (sample T6). The solid line presents the results of the theoretical simulation; the dots are the experimental data. The SHG power is normalized to maximum in symmetrical scheme. Vertical dotted lines on Figs. 8 and 9 are guide for eyes for better comparison of the positions of the reflection minima obtained in the experiments.

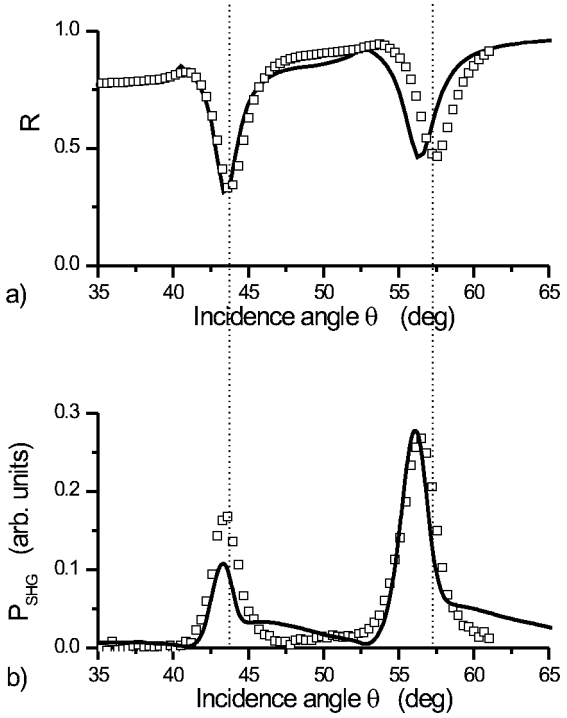

FIG. 9. Same as in Fig. 8 for nonsymmetrical ($\varphi = 96°$) scheme.

these values for the symmetrical scheme of the SEW excitation when $\varphi = 90°$ while Fig. 9 describes the nonsymmetrical scheme when $\varphi \neq 90°$.

The appearance of the well recognizable minimum in the angular dependency R is a criterion of SEW excitation when the phase matching condition at the fundamental frequency is fulfilled. The existence of such a dip in specular reflection is the evidence of a resonant character of SEW excitation; and for the symmetrical scheme it has double resonant character, because SEW resonance may be achieved simultaneously for two angles $\varphi = \pi/2$ and $\varphi = -\pi/2$ as we discussed in Sec. II A.

In general, the width of the SEW resonance in the angular or frequency scale is determined by the SEW damping and the resonance amplitude is proportional to the efficiency of the surface wave launching. The angular θ positions of SEW resonance depend on frequency of light ω and the angle of the grooves orientation φ as it is shown in Fig. 10(a). Taking into account both angles the phase matching conditions can be expressed in the scalar form

$$K_{SEW}^2 = k^2 \sin(\theta)^2 + n^2 q^2 - 2k\, q\, n \sin(\theta) \cos(\varphi),$$

where $k = \omega/c$ and n is the diffraction order. Thus, for a given frequency ω and diffraction order n, φ, and θ are coupled.

For specular reflection in (θ, φ) coordinate space we experimentally observed two crossed dark streaks representing the reflection minima, that indicate the SEW excitation in $+1$ and -1 diffraction orders. For each pair of θ and φ parameters lying on these streaks the phase matching condition is fulfilled. The crossing point of the streaks $\theta_{sym} \approx 50°$ is the region of double resonant SEW excitation specific for the symmetrical scheme $\varphi = \pi/2$, where $\theta_{sym} = \arcsin\sqrt{K_{SEW}^2 - q^2}/k$. If we scan one of the angles in the vicinity of the symmetrical scheme, we should observe consecutively two SEW resonances in ± 1 diffraction orders (Figs. 9 and 10).

In the experiments we observed that the SHG is one order of magnitude more effective in the case of $\theta = \theta_{sym} \pm \delta\theta$ and $\varphi = \pi/2 \pm \delta\varphi$ (''symmetrical scheme'' and ''double resonance'') compared to the other φ values lying over the broad

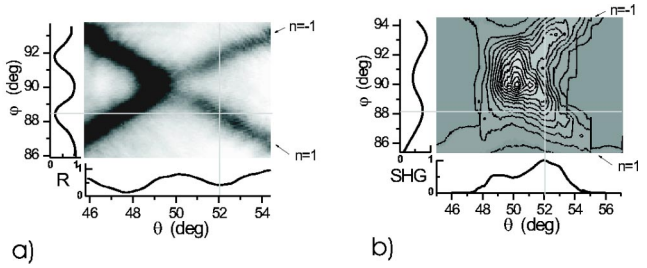

FIG. 10. 2D images of SEW and SHG resonances in (φ, θ) space in the vicinity of symmetrical scheme crossing of $+1$ and -1 orders of diffraction (sample T6). Black color indicates the minimum intensity for s polarization. Gray lines indicate scan direction for φ and θ dependencies, shown on 1D graphs. (a) Specular reflection, ($\lambda = 780$ nm). (b) SHG power ($\lambda = 376$ nm).

range of angle $0<\varphi<\pi/2-\delta\varphi$ [Fig. 10(b)]. However, the efficiency of the SEW excitation in nonsymmetrical scheme is approximately the same for any φ values lying on the dark streaks that show the reflection minimum R_{min} [Fig. 10(a)]. The polarization direction can be optimized at each point along the curve in (θ,φ) space, corresponding to resonance SEW excitation. The width of the SH double resonance is in the range of $\delta\theta=2°$ and $\delta\varphi=3°$ for our gratings.

The enhancement of the reflected signal at the SH frequency in the case of symmetrical scheme is also concerned with the specificity of the SEW excitation geometry. Figure 3(b) shows that two simultaneously excited noncollinear SEW's produce polarization at the SH frequency P_{SH} with a ''short'' wave vector $k^{2\omega}\sin(\Theta_{sym})$ which can radiate straightforwardly into the bulk (air, in our case) in the specular reflection direction. In comparison with the SHG in any other geometry of SEW excitation when $\varphi\neq(\pi/2)n$, the existence of this additional channel of SEW interaction should lead to the sufficient enhancement of nonlinear optical response.

The advantage of the used experimental arrangement is the possibility of simultaneous measurement of the intensity of the waves on the ω and 2ω frequencies versus the angle of incidence θ. It allows us to compare the properties and angular positions of the resonances at both frequencies. We carried out the comparison of angular dependencies of linear reflection $R(\theta,\varphi)$ with nonlinear emission intensity $I_{SHG}(\theta,\varphi)$ for both, symmetrical and nonsymmetrical SEW excitation geometries (Figs. 8 and 9). We paid particular attention on the analysis of mutual angular positions, the relative shapes of SEW and SHG resonances.

In the experiments SH from gold and silver gratings was observed over a broad range of angles of incidence. The range of angles of incidence varied from approximately $\varphi=0°,\theta=19°$ and $\varphi=110°,\theta=65°$ so that the SHG would reach maximum values within this interval for the wide range of φ angles. The shape of the SHG curves versus the angle of incidence and particularly the ratio of SHG maximum to the minimum value of R are sensitive to the set of angle φ. Under the conditions of nonsymmetrical SEW excitation ($\varphi=96°$) we observed two dips in the linear reflection curves that have different relative intensities (Fig. 9). This difference does not correlate with the difference in the efficiency of SEW excitation.

Using the above-developed theoretical approach we may describe the results presented in the experimental chapter of the paper. In all the calculations and theoretical modeling we choose a gold metallic film deposited on the semi-infinite glass substrate with the shape of a grating as the model of the periodic medium (Fig. 5). Upper and lower boundaries of the metallic film are described by the functions: $z_u(y)=H'\sin^2(\pi y/T)$; $z_l(y)=H'\sin^2(\pi y/T)+h$. The theoretical and experimental curves shown on Figs. 8 and 9 are made for the specular reflection of *s*-polarized incoming electric field and reflected SHG has *p* polarization. In the simulation we used the following settings (sample T6): $H'=H^{eff}=80$ nm, $h=35$ nm, $T=1.12$ μm and the wavelength of the laser light is $\lambda=780$ nm, $\epsilon=-21+i1.4$. In the calculations of the nonlinear response of the gold film we used the model of the anharmonism of the free-electron gas.[6] We state the reasonable agreement of the theory with the experiment.

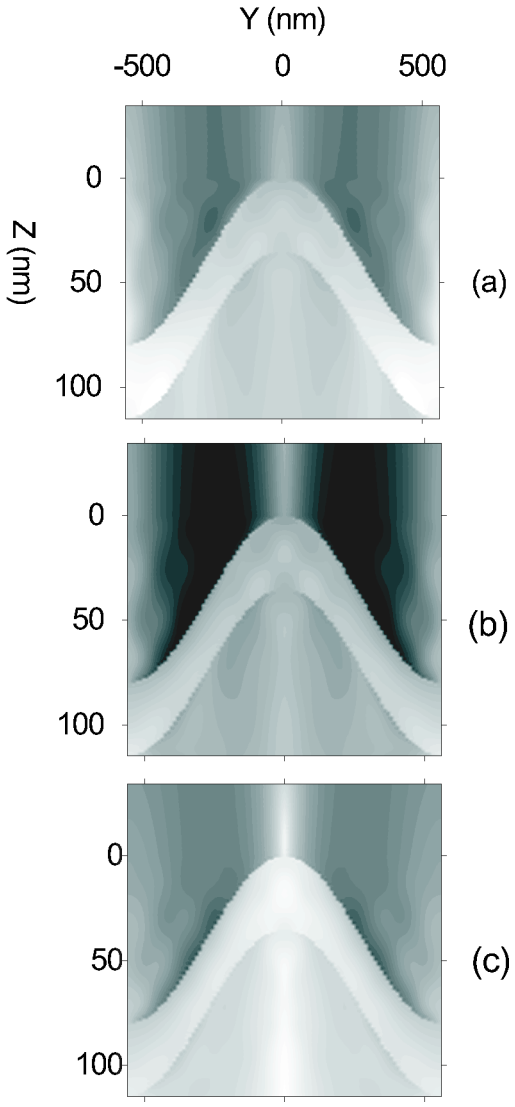

FIG. 11. Electric-field intensity distribution (decimal logarithm of the intensity) around the grating groove, in the air, metal, and substrate for ''symmetrical'' scheme $\varphi=90°$. Black color corresponds to maximum field. (a) Left edge of the SEW resonance ($\theta=47°$), (b) SEW resonance ($\theta=49.20°$), (c) right edge of the SEW resonance ($\theta=53°$).

The above-mentioned theoretical approach may also be used for the description of various nonlinear optical effects that take place on a surface in the presence of SEW. First, we would like to describe the increase of the intensity of SH reflected from the metallic surface with the periodic relief if the exact SEW resonance is achieved. We studied numerically the spatial distribution of the intensity of the total electric field at the fundamental frequency near the surface of the grating. Similar results are presented in other publications,[43,44] but for different grating parameters and geometries.

In Fig. 11 we present the common logarithm of the total electric-field intensity for the azimuth angle $\varphi=90°$ and dif-

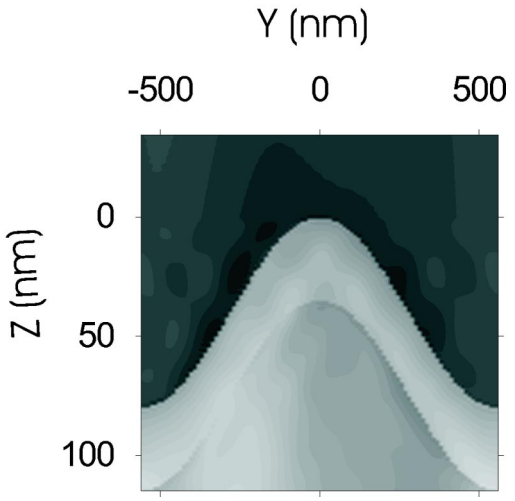

FIG. 12. Same as in Fig. 11 for nonsymmetrical scheme $\varphi = 96°$. SEW resonance ($\theta = 43°$).

ferent incidence angles of the pump beam: $\theta_{sym} = 49.25°$—exact SEW resonance [Fig. 11(b)] and for two angles on the edge of SEW resonance $\theta = 47°$ and $\theta = 53°$ [Figs. 11(a) and 11(c), respectively]. Under the exact resonance conditions the intensity of the total electric field increases approximately five times and the electric field is mainly localized on the side flanks of the grating grooves. Figure 12 shows the spatial distribution of the total electric-field intensity for the fundamental frequency that is assigned to SEW resonance in nonsymmetrical scheme $\varphi \approx 96°$. However, in the case of $\varphi \approx 90°$ the total electric-field intensity is approximately two times larger. The numerical calculations describe well the following intensity and polarization peculiarities: (i) *p* polarization of SHG is originated by the *s* polarization of the pump wave near the main resonance minimum for $\varphi = 90°$; (ii) SHG in symmetrical scheme is several times more intensive than in nonsymmetrical scheme ($\varphi = 96°$); (iii) in nonsymmetrical scheme SHG resonance is shifted to the left slope of SEW resonance.

B. Sum-frequency generation

Later on in Secs. V B and V C we describe the experimental configurations for which it is essential to consider the interaction on the surface of several independently excited SEW's. The configurations of SEW excitation and their interaction were described and discussed in detail in Sec. II B of the paper. In this part of the paper we start the discussion of the nonlinear optical experiments on the generation of signals at the following frequencies $2\omega_1$, $\omega_1 + \omega_2$, and $2\omega_2$. We would like to note that in our experiments the output optical signals at these frequencies had comparable intensities, but according to the phase matching conditions they had a different radiation directions (Figs. 4 and 13). Figures 14 and 15 represent the dependence of the coefficient of the specular reflection *R* versus the angle of incidence θ for a fundamental wavelength $\lambda_1 = 812$ nm and two different values of λ_2: 670 nm in Fig. 14 and 690 nm in Fig. 15. The position of SEW resonance on θ axis in symmetric scheme is

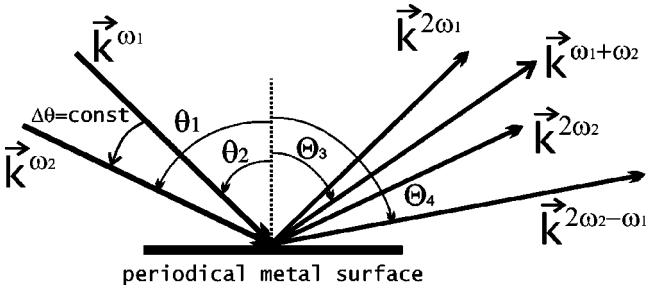

FIG. 13. Directions of the emission of the nonlinear optical signals shown in incidence plane for various two-frequency mixing experiments.

determined by the frequency of the incoming wave according to the following expression $\theta_{sym}(\omega) = \arcsin[c/\omega\sqrt{K_{SEW}^2 + q^2})]$. The angle between beams $\Delta\theta = \theta_{sym}(\omega_2) - \theta_{sym}(\omega_1)$ was chosen in such a way to excite SEW at both frequencies at one grating position. SFG power was measured by scanning incidence angles θ_1 and θ_2 while keeping $\theta_2 - \theta_1 = \text{const}$. The detector position is optimize simultaneously.

From Fig. 14 we can conclude that SF intensity is maximal when the density of local fields due to both SEW's SEW_1 and SEW_2 is the largest. The width of SF resonance is close to the convolutions of widths of SEW_1 and SEW_2 resonances. Angular position of the maximum and the radiation direction of the SF signal are determined by phase matching condition: $\Theta_3 = \arcsin([\sin(\theta_{sym,1}) + \sin(\theta_{sym,2})]/2) \approx (\theta_{sym,1} + \theta_{sym,2})/2$. For a higher fundamental beam frequency ($\omega_2, \lambda_2 = 690$ nm), SEW resonance is wider and less effective then for lower frequency ($\omega_1, \lambda_1 = 812$ nm). This difference is concerned with the higher SEW absorption rate on the metal at high frequencies. At optimal overlapping of areas where SEW's were excited in space and time, nonlinear response at sum frequency $\xi = (I^{\omega_1+\omega_2})/I^{\omega_1} \times I^{\omega_2} = 1.5 \cdot 10^{-20}$ cm^2/W has the same order of magnitude that for SH $\xi = I^{2\omega_1}/(I^{\omega_1})^2 = 2.4 \times 10^{-20}$ cm^2/W. The efficiency of conversion to nonlinear signal is $\eta = (I^{\omega_1+\omega_2})/(I^{\omega_1} + I^{\omega_2}) = 2 \times 10^{-11}$. In this case peak intensity of both fundamental beams was roughly 5 GW/cm^2 (beam waist diameter was in the order of 70 μm) and their average power was 10 mW. We can also estimate the averaged power of the SF wave as 0.3 pW.

C. Four-wave mixing

Finally, we study the effects concerned with the enhancement of the coherent signal at the FWM frequency $\omega_4 = 2\omega_2 - \omega_1$ by the local fields of different SEW's on the grating surface. For the wavelengths used in the experiments $\lambda_1 = 812$ nm, $\lambda_2 = 690$ nm the resulting wave at the FWM frequency was located around $\lambda_4 = 600$ nm. The resulting wavelength and the angular location of the signal maxima are determined by the phase matching conditions as one can see from Figs. 4(b) and 15. Unlike previously discussed processes, FWM is nonlinear process of third order by field, but nevertheless according to our observations the intensity of the resulting wave at the FWM frequency exceeded the in-

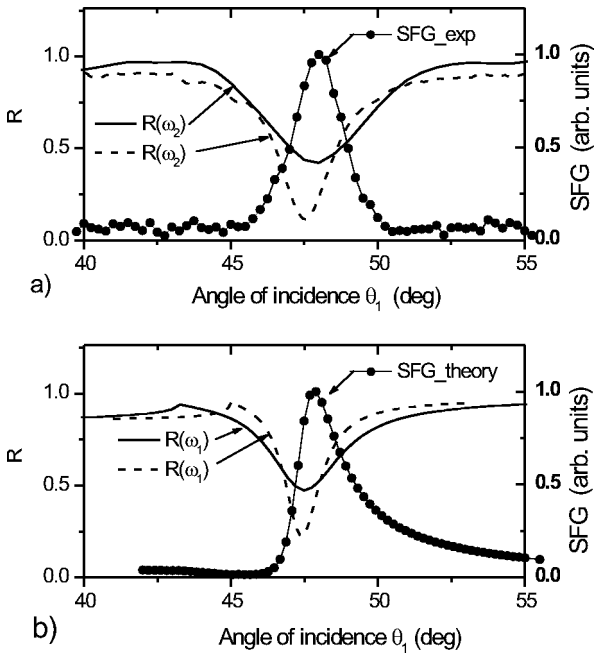

FIG. 14. Angular dependences of the reflectivity R and the SFG intensity in the presence of SEW resonance. Angle between beams ω_1 and ω_2 is fixed at $\theta_1-\theta_2=\Delta\theta$, $\lambda_1=812$ nm, $\lambda_2=670$ nm, $\Delta\theta=11°$, $\varphi=90°$. The signal on the SF is detected at the direction $\Theta_1+\Delta\Theta_{SFG}$: (a) experiment (sample B2), (b) theory (sample B2).

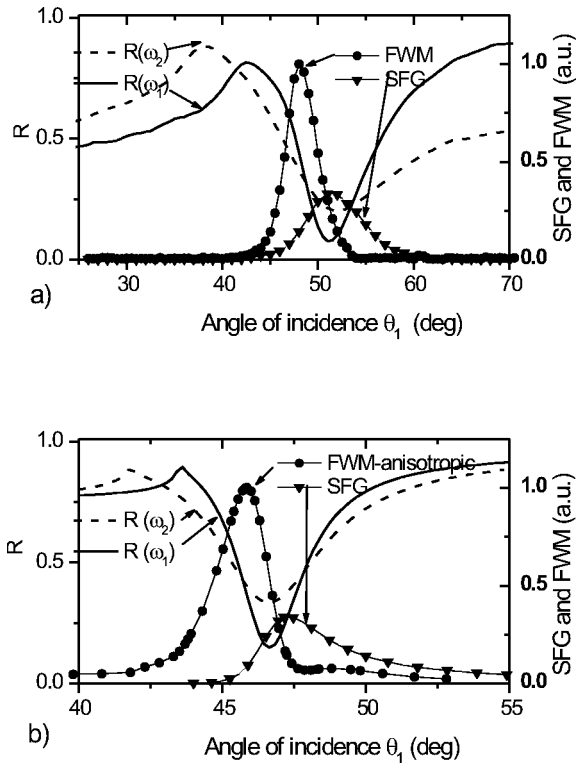

FIG. 15. Mutual position of SEW resonances and nonlinear signal maxima. Angle between beams ω_1 and ω_2 is constant $\theta_1-\theta_2$. $\lambda_1=812$ nm, $\lambda_2=690$ nm, $\Delta\theta=14°$, $\varphi=90°$. Nonlinear signal is detected in another direction $\Theta_1+\Delta\Theta_{SFG}$, $\Theta_1+\Delta\Theta_{FWM}$. (a) Experiment (sample M9), (b) theory (sample T6).

tensity of SHG and SFG (Fig. 16). The efficiency of the conversion into the FWM intensity $\eta=(I^{2\omega_2-\omega_1})/(I^{\omega_1}+I^{\omega_2})=5\times10^{-11}$ and nonlinear response was $\xi=(I^{2\omega_2-\omega_1})/I^{\omega_1}(I^{\omega_2})^2=1.8\times10^{-30}$ cm^4/W^2.

VI. CONCLUSIONS

To draw a conclusion, we would like to note several specific properties of the nonlinear optical signals that we observed in the experiment and described theoretically:

(1) The first remark is concerned with the polarization properties of different interacting waves depicted in Figs. 3 and 4. As we described in Secs. II and III of this paper the SEW's are always p polarized for all incoming laser beams on the fundamental frequencies. However because we used noncollinear interacting SEW's, all the incoming fundamental beams have s polarization. In our symmetric scheme the output nonlinear optical signals may have different polarizations. For instance, both SH and SF waves have p output polarization (see also Ref. 45) , whereas the FWM wave has at the same time s output polarization. We didn't especially investigate the effects concerned with the polarization self-actions and their participation of the SEW's, but in literature such effects were already described theoretically.[5] However, in spite of the fact that we didn't observe clearly the polarization conversion and self-action effects we understand well that along with the spatial and temporal pulse overlapping, the set of proper wave polarizations is also essential for the nonlinear optical conversion efficiency optimization.

(2) For the two-frequency experiments under the different emission angles one may observe simultaneous generation of four nonlinear optical signals as it is shown in Fig. 13. For instance, in Fig. 4(a) it is shown that there are two equal possibilities determined by the phase matching conditions for the SHG at ω_1 and ω_2 frequencies. However, at the same time SHG_2 signal is weaker than SHG_1 in Fig. 16. Closer effects have already been described in Refs. 9,10 and we believe that they are concerned with the decrease of the local electromagnetic field because of a weaker SEW resonance for the higher frequency of electromagnetic field of the laser light. However, we would like to note that the intensity of different nonlinear signals increases for longer wavelength. Experiments for SHG, SFG, and FWM were held for differ-

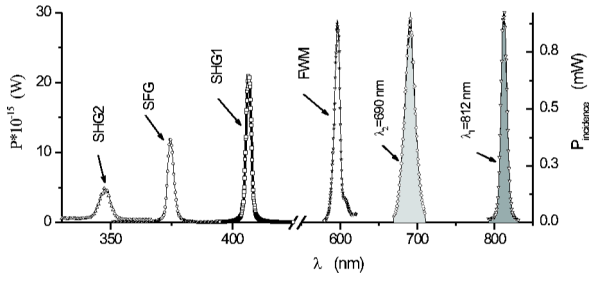

FIG. 16. Spectra of all interacting waves. Incidence angles are $\theta_1=52°$, $\theta_2=66°$, $\varphi_1=\varphi_2=90°$. Filled areas indicate waves at fundamental frequencies. Signals are measured in dirrections indicated in Fig. 13 (sample M9).

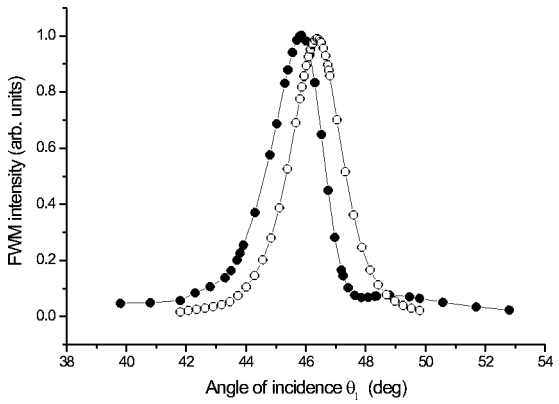

FIG. 17. Results of the theoretical modeling for FWM in the assumption of the isotropic (opened dots) and anisotropic material of the grating (dark dots). Sample T6.

ent materials of gratings, for gold (sample M9, T6) and for silver (sample B2), for different wavelengths ($\lambda = 670 - 830$ nm), pulse durations ($\tau = 60 - 400$ fs) and gave qualitatively similar results. The presented experimental scheme also allows us to study temporal and spatial properties of SEW interaction.[10]

(3) One of the aims of the work was to demonstrate that the theoretical model described above is also applicable for the qualitative description of various nonlinear optical processes. We demonstrated it on the example of SHG, SFG, and FWM process. As an example, we simulated these processes for one of our samples with a simplest spatial profile (sample T6) and obtained a reasonable agreement with the experiment.

(4) It is interesting to note that FWM process agrees well with experiment only if we consider that bulk nonlinear processes are dominant compared with the surface one. Moreover, the good agreement with the experimental data is observed if the properties of the bulk are assumed to be anisotropic in reciprocal lattice vector direction. For isotropic bulk metal FWM maximum would be located at the center of SEW resonance, but in experiment, we clearly observed a noticeable shift of FWM maximum to the short angle edge of SEW resonance (Figs. 15 and 17).

ACKNOWLEDGMENTS

We appreciate the useful discussions with Professor Yu. E. Lozovik and Professor S. N. Seminogov. A.P.S. would like to thank the Université du Littoral for the financial support during the course of these experiments. This work was supported in part by the Russian Foundation for Basic Research (Grants Nos. 01-02-17314, 02-02-17138), BMBF (Grant No. 0081/99 13N7516) and ''Universities of Russia''(Grant No. UR.01.03.001). The Laboratoire de Physico Chimie de l'Atmosphère participates with the Centre d'Etude et de Recherche Lasers et Applications, supported by the Ministère de la Recherche, the Région Nord Pas de Calais, France, and the Fond Européen de Développement Economique des Régions.

*Electronic address: alex@lasmed.phys.msu.su

[1] H. Raether, *Surface Plasmons on Smooth and Rough Surfaces and on Gratings* (Springer-Verlag, Berlin, 1988), Vol. 111.
[2] V. M. Shalaev, *Nonlinear Optics of Random Media: Fractal Composites and Metal-Dielectric Films*, Springer Tracts in Modern Physics, Vol. 158 (Springer, Berlin, 2000).
[3] R.W. Wood, Philos. Mag. **4**, 396 (1902).
[4] R. Petit, *Electromagnetic Theory of Gratings* (Springer, Berlin, 1989).
[5] A.V. Kats and I.S. Spevak, Phys. Rev. B **65**, 195406 (2002).
[6] Y. R. Shen, *The Principles of Nonlinear Optics* (Wiley, New York, 1984).
[7] S. A. Akhmanov and R. V. Khokhlov, *Problems of Nonlinear Optics* (VINITI, Moscow, 1964).
[8] N. Bloembergen, *Nonlinear Optics* (Benjamin, New York, 1965).
[9] Yu.E. Lozovik, S.P. Merkulova, M.M. Nazarov, and A.P. Shkurinov, Phys. Lett. A **276**, 127 (2000).
[10] Yu.E. Lozovik, S.P. Merkulova, M.M. Nazarov, A.P. Shkurinov, and P. Masselin, JETP Lett. **75**, 461 (2002).
[11] M. Kreiter, S. Mittler, W. Knoll, and J.R. Sambles, Phys. Rev. B **65**, 125415 (2002).
[12] Yu.E. Lozovik, M.M. Nazarov, and A.P. Shkurinov, Phys. Scr. **60**, 60 (1999).
[13] A.V. Andreev, A.V. Balakin, A.B. Kozlov, I.A. Ozheredov, I.R. Prudnikov, A.P. Shkurinov, P. Masselin, and G. Mouret, J. Opt. Soc. Am. B **19**, 1865 (2002).
[14] A.V. Andreev, A.V. Balakin, A.B. Kozlov, I.A. Ozheredov, I.R. Prudnikov, A.P. Shkurinov, P. Masselin, and G. Mouret, J. Opt. Soc. Am. B **19**, 2083 (2002).
[15] A.V. Balakin, D. Boucher, V.A. Bushuev, N.I. Koroteev, B.I. Mantsyzov, P. Masselin, I.A. Ozheredov, and A.P. Shkurinov, Opt. Lett. **24**, 793 (1999).
[16] A.V. Balakin, V.A. Bushuev, B.I. Mantsyzov, I.A. Ozheredov, E.V. Petrov, A.P. Shkurinov, P. Masselin, and G. Mouret, Phys. Rev. E **63**, 046609 (2001).
[17] N. Blombergen, R.K. Chang, S.S. Jha, and C.H. Lee, Phys. Rev. **174**, 813 (1968).
[18] J.-L. Coutaz, M. Neviere, E. Pic, and R. Reinisch, Phys. Rev. B **32**, 2227 (1985).
[19] J.-L. Coutaz, J. Opt. Soc. Am. B **4**, 105 (1987).
[20] H.J. Simon and Zhan Chen, Phys. Rev. B **39**, 3077 (1989).
[21] M. Neviere, R. Reinisch, and D. Maystre, Phys. Rev. B **32**, 3634 (1985).
[22] H.R. Jensen, R. Reinisch, and J.-L. Coutaz, Appl. Phys. B: Lasers Opt. **64**, 57 (1999).
[23] R. Reinisch, M. Neviere, E. Popov, and H. Akhoulayri, Opt. Commun. **112**, 339 (1994).
[24] A.C.R. Pipino, G.C. Schatz, and R.P. Van Duyne, Phys. Rev. B **49**, 8320 (1994).
[25] A.C.R. Pipino, G.C. Schatz, and R.P. Van Duyne, Phys. Rev. B **53**, 4162 (1996).
[26] A.A. Kovalev, P.S. Kondratenko, A.A. Liberman, and B.N. Levinskii, Tech. Phys. **38**, 577 (1993).
[27] P.S. Kondratenko, Sov. J. Quantum Electron. **16**, 1326 (1986).
[28] J. Bereiter-Hahn, C. Blase, Yu.E. Lozovik, M.M. Nazarov, and

A.P. Shkurinov, Sov. J. Quantum Electron. **33**, 451 (2003).
[29] G.S. Agarwal and S.S. Jha, Phys. Rev. B **26**, 482 (1982).
[30] G.A. Farias and A.A. Maradudin, Phys. Rev. B **30**, 3002 (1984).
[31] P. Petruskevicius, Phys. Status Solidi A **175**, 207 (1999).
[32] A.A. Angeluts, A.A. Goncharov, N.I. Koroteev, I.A. Ozheredov, and A.P. Shkurinov, Sov. J. Quantum Electron. **27**, 64 (1997).
[33] V.N. Seminogov and A.I. Khudobenko, Sov. Phys. JETP **69**, 284 (1989).
[34] S. A. Akhmanov, V. I. Sokolov, V. N. Seminogov, and V. Ya. Panchenko, *Interaction of Super-short Laser Pulses with Targets having Periodic Surface Relief, Itogi Nauki i Tekhniki, Ser. Sovremennye Problemy Lazernoy Fiziki*, Vol. 4, p. 199 (VINITI, Moscow, 1991) (in Russian).
[35] V.N. Seminogov and V.I. Sokolov, Opt. Spectrosc. **68**, 50 (1990).
[36] Y.-Y. Teng and E. Stern, Phys. Rev. Lett. **19**, 511 (1967).
[37] M. M. Nazarov, Ph.D. dissertation, M. V. Lomonosov Moscow State University, 2002.
[38] C.G. Darwin, Philos. Mag. **27**, 675 (1914).
[39] M. Born and E. Wolf, *Principles of Optics* (Pergamon, New York, 1964).
[40] L. D. Landau and E. M. Lifshitz, *The Classical Theory of Fields* (Pergamon, Oxford, 1994).
[41] L.G. Parratt, Phys. Rev. **95**, 359 (1954).
[42] Yu.N. Barabanenkov and V.L. Kuznetsov, J. Commun. Technol. Electron. **44**, 614 (1999).
[43] M. Kreiter, T. Neumann, S. Mittler, W. Knoll, and J.R. Sambles, Phys. Rev. B **64**, 075406 (2001).
[44] R.A. Watts, T.W. Preist, and J.R. Sambles, Phys. Rev. Lett. **79**, 3978 (1997).
[45] E.W.M. van der Ham, Q.H.F. Vrehen, E.R. Eliel, V.A. Yakovlev, E.V. Alieva, L.A. Kuzik, J.E. Petrov, V.A. Sychugov, and A.F.G. van der Meer, J. Opt. Soc. Am. B **16**, 1146 (1999).